Size-dependent magnetic spin and orbital moments of Fe nanoparticles deposited onto Co/W(110)

A. Kleibert* and K.-H. Meiwes-Broer
Institut für Physik, Universität Rostock, D-18051 Rostock, Germany

J. Bansmann
Institut für Oberflächenchemie und Katalyse, Universität Ulm, D-89069 Ulm, Germany

(Received 19 September 2008; revised manuscript received 25 February 2009; published 23 March 2009)

In situ x-ray magnetic circular dichroism (XMCD) measurements by means of total electron-yield detection have been carried out on mass-filtered Fe nanoparticles with diameters ranging from 6 to 10 nm upon deposition onto Co/W(110). The shape as well as the crystallographic structure has independently been investigated by means of high-resolution transmission electron microscopy. An evaluation of the XMCD spectra revealed bulklike magnetic spin moments but strongly enhanced magnetic orbital moments after correcting for electron-yield saturation effects. The observed size dependence of the magnetic moments cannot be understood in simple core shell models where the core is assumed to be bulklike and only the outer shell possesses enhanced values according to their reduced coordination at the surface. Instead, size-dependent distortions of the crystal lattice due to surface and interfacial tension as well as mesoscopic relaxations at the surface facets of the nanoparticles are considered as the origin of the observed large orbital moments.

DOI: 10.1103/PhysRevB.79.125423 PACS number(s): 61.46.Df, 61.05.cj, 75.50.Bb, 75.70.Rf

I. INTRODUCTION

Clusters and nanoparticles (NPs) are small fragments of matter that possess unique and size-dependent properties not known from their atomic constituents or the corresponding bulk.[1] In particular, the remarkable size dependence of the magnetic properties of small 3*d* transition-metal clusters has attracted much attention.[2–4] Due to their high surface-to-volume ratio and the reduced coordination, these particles show strongly enhanced magnetic moments up to about 500–1000 atoms per cluster. Similarly, in supported clusters enhanced magnetic spin and orbital moments have been reported.[5–10] The existence of giant magnetic anisotropy was found in the case of small Co clusters supported by Pt(111).[11] From these experiments, one may conclude that larger particles will generally show almost bulklike magnetic anisotropy and moments. But besides low coordination effects at the surface of clusters, the inner structure and the shape of the cluster are also decisive for their magnetic properties.[12] When increasing the size of clusters complex structural phase transitions occur, typically starting from noncrystalline icosahedral configurations and ending up with the crystalline structure known from bulk matter.[13–15] However, even large nanoparticles (consisting of several tens of thousand atoms) can exist in metastable states, e.g., crystallographic structures being significantly different from the bulk with consequences to their magnetic properties.[12,16] Surface tension may additionally act on their crystal structure, and thus, on the properties of the nanoparticles.[17] The presence of a substrate may furthermore modify the structure of the particle via additional interfacial contact forces.

In this paper, we report on the magnetic spin and orbital moments of comparably large Fe nanoparticles consisting of 14 000 up to 50 000 atoms. These nanoparticles have been generated in the gas phase by using an arc cluster-ion source (ACIS) and subsequently deposited mass-filtered under soft-landing conditions onto epitaxially ordered ultrathin Co(0001) films on W(110).[18–20] In order to understand their magnetic properties, the knowledge of the crystallographic structure and the shape of the nanoparticles is important as recently reported.[21] Therefore, this study combines (i) a structural analysis via high-resolution transmission electron microscopy (HRTEM) and (ii) a magnetic analysis using x-ray absorption spectroscopy (XAS) and x-ray magnetic circular dichroism (XMCD) in the vicinity of the Fe $L_{2,3}$ edges.

XMCD is a powerful tool that enables element-specific determination of magnetic spin and orbital moments, separately, by means of magneto-optical sum rules.[22,23] However, from thin-film studies it is well known that total electron-yield (TEY) detection suffers from electron-yield saturation effects when the penetration depth of the incoming x rays becomes small relative to the finite escape length of the excited electrons.[24] As a result, magnetic moments obtained from sum-rule analysis of TEY measurements are generally underestimated. Additionally, a distinct surface sensitivity results from the finite escape depth. In the case of plane surfaces or thin films, the influence of saturation effects can easily be corrected.[25,26] Electron-yield saturation in respective experiments on supported nanoparticles has recently been studied by Monte Carlo simulations, and it turned out that it requires attention for particles being larger than about 3 nm.[27] Accordingly, we have performed corresponding calculations for Fe particles over a wide size range with particular emphasis on the surface sensitivity of the TEY signal. Based on these calculations our experimental findings on the magnetic spin and orbital moments are analyzed and discussed.

This paper is organized as follows. In Sec. II we describe the experimental setup for sample preparation and the XMCD investigations. Additionally, we briefly discuss the properties of the Co(0001)/W(110) substrates as far as it is relevant for this work; details regarding Fe(110) films on W(110) are given in previous publications.[28,29] The shape and structure of the Fe nanoparticles are discussed on the basis of independent HRTEM investigations in Sec. III. XMCD spectroscopy has been described many times and

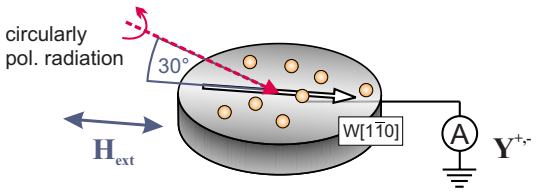

FIG. 1. (Color online) Experimental setup for the XMCD experiments. Circularly polarized synchrotron radiation impinged at an angle of 30°. External magnetic field pulses were applied along the magnetic easy axis of the sample being in the scattering plane. Absorption spectra have been recorded by means of total electron detection.

thus we refer to the literature (for an overview, see Refs. 22, 30, and 31). In the following, a detailed analysis of the absorption spectra, TEY-induced saturation, and escape depth effects as well as a simulation of the Fe nanoparticle absorption spectra is presented. Finally, using the obtained correction factors, the magnetic spin and orbital moments of mass-filtered Fe nanoparticles on Co films are shown and discussed with respect to theoretical data and recent experimental findings.

II. EXPERIMENTAL DETAILS

Fe nanoparticles have been generated using a home-built arc cluster-ion source.[18] The ACIS is designed to provide a high flux of mass-filtered metallic pure or alloy nanoparticles with diameters between 4 and 15 nm.[19,20] A large fraction of the particles being preformed in the gas phase is singly charged. An electrostatic quadrupole enables the separation of mass-filtered clusters from the beam originally having a broad size distribution. Respective ensembles of mass-filtered particles show a narrow size distribution with $\Delta D/D \sim 0.12$, where D is the mean particle diameter and ΔD represents the width of a fitted Gaussian distribution.[32] The ACIS allows for *in situ* deposition under soft-landing conditions with the kinetic energy of the particles being smaller than 0.1 eV/atom. In the present experiments mass-filtered Fe nanoparticles have been deposited onto epitaxially grown ultrathin hcp(0001) Co films on W(110). The particle density on the samples has been chosen low enough to avoid agglomeration and allowing for investigations on an ensemble of individual nanoparticles. The Co films provide a well-defined and atomically flat support for the nanoparticles; the exchange field at the interface allows for a remanent alignment of the magnetic moments of the nanoparticles.[33] The uniaxial in-plane anisotropy of the films enables a well-controlled magnetization along the magnetic easy axis being parallel to the W[1$\bar{1}$0] direction (cf. Fig. 1).[34,35]

The W(110) substrates have been cleaned by cycles of heating in oxygen atmosphere as described in the literature.[36,37] Co(0001) films with a thickness of about 13 monolayers (MLs) were prepared by means of electron-beam evaporation at room temperature with a rate of about 0.7 atomic MLs per minute. Atomically flat film surfaces were obtained after annealing the films at 370 K for several minutes.[37] The cleanliness and quality of the substrate and film surfaces have been checked by means of low-energy electron diffraction. During the preparation, the base pressure did not exceed 5×10^{-10} mbar. During the nanoparticle deposition, however, the pressure in the preparation chamber temporarily increased up to 1×10^{-6} mbar due to the high amount of rare gases (Ar or He) being involved in the cluster generation and rapidly decreased after the deposition. Fe(110) films on W(110), which have been used for comparing the absorption data, have been prepared similar to the Co films, details are given in Refs. 28 and 29 and references therein.

The XMCD experiments were carried out at the undulator beamline UE56/1 PGM at the electron storage ring BESSY (Berlin). We may note that in a previous experiment on Co/W(110), the limited photon flux and x-ray beam stability did not allow us to determine the spin and orbital moments, separately, from the photoabsorption spectra.[33] With a revised experimental setup at the undulator beamline, spectra have been measured at a fixed helicity while switching the magnetization of the samples. Accordingly, the improved data quality enabled us to obtain the spin and orbital moments separately and also provided a more reliable determination of the orbital to spin moment ratio when compared to Ref. 33. The degree of circular polarization was $P_c \sim 0.9$ in the required energy range of 690–815 eV. The radiation impinged at an angle of 30° with respect to the sample surface. The sample was oriented with the easy magnetization axis parallel to the plane of incidence. For the XMCD spectra a short magnetic field pulse of about 100 mT has been applied in order to switch the magnetization of the samples at each photon energy. X-ray absorption spectra were recorded in remanence by means of total electron-yield detection. The spot size was about 200×200 μm^2. All experiments have been carried out at room temperature.

III. SHAPE AND ATOMIC STRUCTURE OF Fe NANOPARTICLES

The shape and structure of Fe nanoparticles have been investigated independently by means of HRTEM. Images of two different Fe nanoparticles embedded in an aluminum matrix are shown in the upper panels of Fig. 2. The particle diameters D are about 13 nm in (a) and 7.5 nm in (b). Quantitative analysis of the images reveals, in both cases, pure Fe with a lattice constant of 2.87 Å. Atomically resolved areas are marked by white frames and depicted enlarged in the insets. The atomic planes visible in the inset of Fig. 2(a) correspond to (110) planes of the bcc Fe lattice. The particle is thus oriented with a [001] axis parallel to the electron beam. In Fig. 2(b) the crystal lattice is aligned with the [112] axis perpendicular to the paper plane.

The edges and vertices being visible in Fig. 2(a) account for a truncated rhombic dodecahedron showing 12 quasihexagonal (110) and 6 quadratic (001) facets. Corresponding contours of the particles in Figs. 2(a) and 2(b) are outlined by white lines in panels (c) and (d), the black circles mark equivalent positions and serve as a guide for the eyes. The shape as well as the atomic structure of nanoparticles may, in general, deviate from its energetically favorable configura-

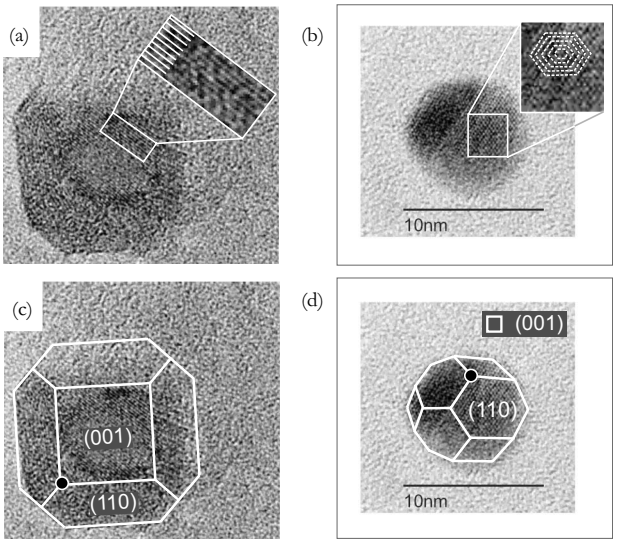

FIG. 2. Top: HRTEM images of two different Fe nanoparticles being embedded in an Al matrix. The particles have diameters D of about 13 nm in (a) and 7.5 nm in (b). Atomically resolved areas marked by the white frames are enlarged in the insets. Bottom: the same particles together with the corresponding contours of their shape are given in (c) and (d), respectively.

tion due to kinetic barriers in the cluster formation process.[13,38,39] However, the same shape has been reported by Vystavel *et al.* after deposition of Fe nanoparticles onto carbon films and *in situ* annealing under high-vacuum conditions in Ref. 40. In the following we will assume that the Fe nanoparticles generated by the ACIS are close to the thermodynamic equilibrium state being predicted by Wulff's theorem.[41] Indication for partial flattening has been found upon deposition of the iron nanoparticles onto the bare W(110) surface and is ascribed to the higher surface energy of tungsten relative to iron.[21] However, due to the nearly identical surface energy of Fe and Co and kinetic barriers hindering significant material transport at room temperature, we expect that the nanoparticle shape is almost preserved or only slightly modified upon deposition onto the Co films on W(110).[42]

IV. X-RAY ABSORPTION SPECTRA AND DATA ANALYSIS

Total electron-yield spectra of a sample with mass-filtered Fe nanoparticles with $D=7.6\pm1.5$ nm on top of a 13 ML Co film are shown in Fig. 3. The given energy range covers the $L_{2,3}$ edges of both elements, Fe as well as Co. Dashed red and solid black lines depict spectra recorded with opposite sample magnetization (denoted as Y^+ and Y^-, respectively). The present intensity difference (XMCD) hints toward magnetic saturation of the sample in remanence as confirmed by the sum-rule application below. On the left-hand side of Fig. 3, the absorption intensity recorded at the Fe $L_{2,3}$ edges (at 705 and 718 eV) is much smaller when compared to the Co film (at 775 and 790 eV), reflecting the comparably low Fe particle density on the sample. The Fe features are shown enlarged in the inset. After subtracting the separately recorded background spectra Y^b (solid gray lines), the edge

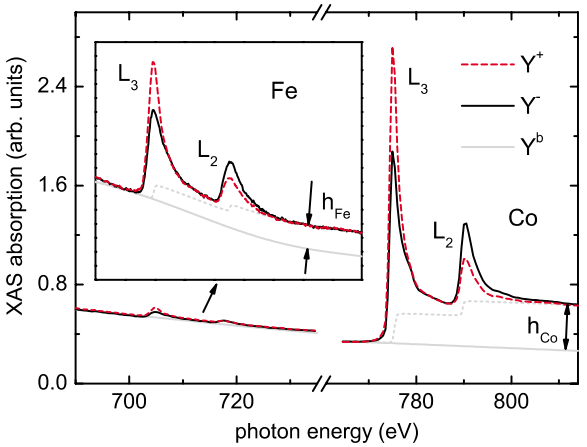

FIG. 3. (Color online) X-ray absorption spectra in the vicinity of the $L_{2,3}$ edges of Fe nanoparticles with $D=7.6\pm1.5$ nm deposited on Co(0001) films with a thickness of about 13 ML. The Fe spectra are enlarged in the inset.

jump ratio evaluates to $h_{Co}/h_{Fe}\sim30$. From the known Co film thickness of about 13 ML, an equivalent Fe thickness of 0.4 ML can be estimated. Assuming a spherical shape of the Fe particles with $D=7.6$ nm and bulklike atomic density, this results in a coverage of about 200 particles per μm^2, in agreement with independent deposition experiments.[43] The corresponding mean cluster-cluster distance is about 80 nm and thus allows for investigations on ensembles of individual particles.

A quantitative analysis of x-ray absorption spectra has been carried out as outlined by Chen *et al.*[31] The left panel of Fig. 4 shows the isotropic photoabsorption spectrum of the nanoparticles given by $Y^0=Y^+ + Y^-$ (dashed red lines). This total electron yield is displayed together with absorption spectra $\mu^0=\mu^+ + \mu^-$ of a 13 ML Fe film on W(110) (solid black lines). The latter are TEY data corrected for saturation effects. In a previous study it was found that similar films show almost bulklike isotropic spectra.[35] Thus, the corrected film data in the left panel of Fig. 4 may serve as bulklike reference spectrum. The comparison yields a significantly reduced L_3 peak of the nanoparticle spectra with respect to the Fe film data. In the present size regime such a decrease can barely be ascribed to an altered occupation of the $3d$

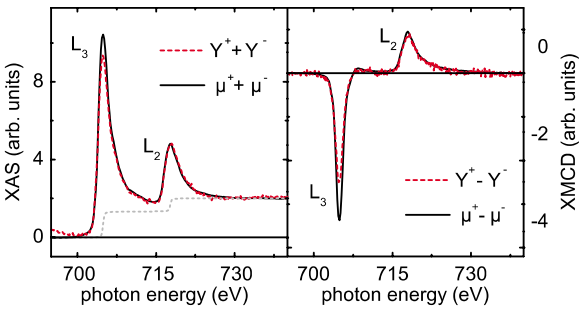

FIG. 4. (Color online) Left: isotropic spectrum of Fe nanoparticles ($Y^+ + Y^-$) recorded by means of TEY and an Fe film spectrum after correction of saturation effects ($\mu^+ + \mu^-$). Right: corresponding difference spectra.

TABLE I. Effective magnetic spin moments $m_{\mathrm{spin}}^{\mathrm{eff}}$ and orbital moments m_{orb} of Fe NPs, an Fe film on W(110) (corrected for saturation effects), and Fe bulk.

	7.6 nm NP (uncorrected)	13 ML Fe/W(110) (corrected)	Bulk
$m_{\mathrm{spin}}^{\mathrm{eff}}(\mu_B)$	2.05 ± 0.06	2.11 ± 0.03	1.98
$m_{\mathrm{orb}}(\mu_B)$	0.09 ± 0.02	0.14 ± 0.01	0.085

states relative to bulk iron, cf. also Ref. 44. Instead, we will show below that the apparently reduced peak intensity is caused by the saturation effects in the total electron-yield detection.[26,27]

The right panel of Fig. 4 depicts the corresponding difference spectra $Y^+ - Y^-$ and $\mu^+ - \mu^-$, respectively, containing the magnetic information. Both data sets are corrected for the finite degree of circular polarization and the angle of 30° between the magnetization and the propagation axis of the radiation. For single crystalline samples the application of the orbital sum rule yields in general anisotropic orbital moments when the magnetization is oriented along distinct directions.[45,46] The magnetic orbital moment is largest when aligning the magnetization parallel to the magnetic easy axis.[46,47] Similarly, the anisotropic spin density enters the analysis via the so-called dipole term m_T. As a consequence the effective spin moment $m_{\mathrm{spin}}^{\mathrm{eff}} = m_{\mathrm{spin}} + 7m_T$ is obtained when applying the spin sum rule.[30,46,48] In the case of Fe the dipole term contribution $7m_T$ is of the order of $0.1-0.2\mu_B$ and leads to a respective enhancement $m_{\mathrm{spin}}^{\mathrm{eff}}$ when the magnetization is pointing along the magnetic easy axis.[49] For Fe films epitaxially grown on W(110) a sizeable strain- and interface-induced magnetocrystalline anisotropy is well known.[50,51] Accordingly, we obtain an effective spin moment of $m_{\mathrm{spin}}^{\mathrm{eff}} = (2.11 \pm 0.03)\mu_B$ and an orbital moment of $m_{\mathrm{orb}} = (0.14 \pm 0.01)\mu_B$ with the magnetization parallel to the magnetic easy axis (being parallel to W[$1\bar{1}0$]).[52] Both values are enhanced when compared to the isotropic bulk values, cf. Table I. In contrast, the nanoparticle spectra reveal almost bulklike values for the spin and orbital moments as given in Table I. This might partially be due to the presumed random orientation of the particles resulting in a vanishing contribution of the dipole term and the averaging of the orbital moments. However, we will show that saturation effects in the TEY spectra of particles in the present size regime lead to a significant reduction in the magnetic orbital moments when applying the sum rule.

V. SIMULATION OF TEY SPECTRA OF DEPOSITED NANOPARTICLES

In total electron-yield experiments it is assumed that the intensity of the detected drain current is proportional to the absorption coefficient of the sample under investigation. However, saturation effects may lead to significant deviations of the measured signal when compared to the actual photoabsorption cross section.[26,27] In the case of thin film or bulk samples analytic descriptions of the TEY are available that can be used for appropriate corrections. Additionally, the finite escape depth λ_e of the excited electrons plays an important role when investigating nanoparticles with diameters being larger than or comparable to λ_e. In these cases the inherent surface sensitivity of the TEY measurements determines the fraction of the atoms that are probed in the experiment.

In previous simulations on the TEY of deposited Co nanoparticles it was shown that electron-yield saturation effects result in a significant reduction in the measured magnetic orbital moment for particles with $D > 3$ nm.[27] At the same time the magnetic spin moments are also affected and show slightly reduced values. However, Fe possesses larger absorption coefficients at the L edges when compared to Co. Moreover, the effective electron escape depth in TEY experiments is noticeably smaller for Fe ($\lambda_e^{\mathrm{Fe}} = 1.7$ nm) relative to that of Co ($\lambda_e^{\mathrm{Co}} = 2.5$ nm).[26] Accordingly, the results of Ref. 27 cannot be directly transferred to Fe nanoparticles. Respective calculations are presented below.

A. TEY of deposited nanoparticles

Simulations of the TEY have been carried out for spherical Fe nanoparticles with diameters over a wide range. The total electron yield Y of a nanoparticle is given by

$$Y(E) \propto \int_V \mu(E) I(E,\mathbf{r}) W(\mathbf{r}) dV, \tag{1}$$

where $\mu(E)$ is the photon energy-dependent absorption coefficient, $I(E,\mathbf{r})$ is the local radiation intensity, and $W(\mathbf{r})$ is the probability of detecting an electron being excited at position $\mathbf{r}$ within the nanoparticle. The integration is carried out over the particle volume V. For these calculations the bulklike (corrected) absorption coefficients $\mu(E)$ of the Fe film on W(110), cf. Fig. 4, have been used as well as perpendicularly incident x rays have been assumed. For two particles with diameters of 12 and 6 nm, the local radiation intensity and the probability of electron emission as determined from the simulations are shown in Fig. 5. Details of the calculation are presented in the Appendix.

The radiation intensity distribution $I(E,\mathbf{r})$ within the particles is calculated for the photon energy being set to the Fe L_3 peak. The gray level legend at the bottom denotes the intensity relative to the incoming radiation, and thus brighter levels correspond to higher intensities. The attenuation length (~20 nm) is not limiting the information depth of the experiment. The right column of Fig. 5 illustrates the probability $W(\mathbf{r})$ to detect an electron that has been generated at $\mathbf{r}$ (lighter gray tones correspond to higher probability as stated in the legend below). The probability to detect an excited electron in a TEY measurement is determined by two factors. (i) The probability that an electron may leave the particle along a certain linear trajectory is damped exponentially with a characteristic scattering length. (ii) Without the presence of a substrate the probability of detecting an electron only depends on the distance between the particle center and the excitation point of the electrons motion. Thus $W(\mathbf{r})$ would be isotropic with the smallest value in the particle center while electrons from the surface would contribute with $W(\mathbf{r}) = 1$ to

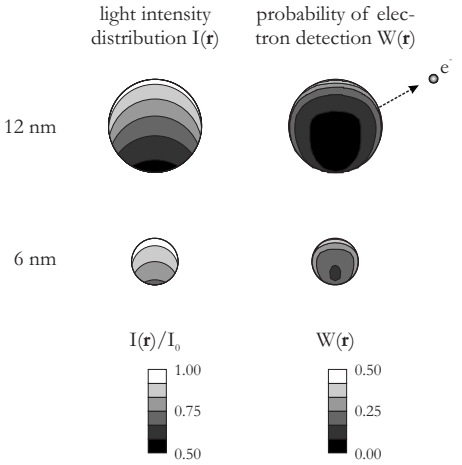

FIG. 5. Light intensity distribution (left) and probability of electron emission (right) of two spherical Fe nanoparticles. The upper (lower) particle has a diameter of 12 nm (6 nm). Bright gray tones denote high and dark ones denote low values as indicated.

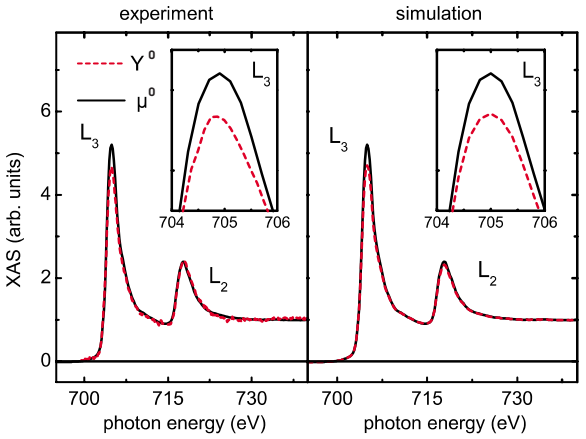

FIG. 6. (Color online) Left: experimentally determined isotropic spectra of Fe nanoparticles with $D=7.6\pm1.5$ nm together with the corrected Fe film data (solid black line). Right: simulated total electron-yield spectra of spherical nanoparticles (red dashed line) based on the corrected Fe film data (solid black line).

the detected TEY. In the experiments presented here, the particles are deposited onto a substrate, which absorbs electrons scattered into the lower half space, and the isotropic symmetry of $W(\mathbf{r})$ of a free particle is reduced. In the right column of Fig. 5, the substrate-induced anisotropy of $W(\mathbf{r})$ is visible in both particles. As a consequence, even electrons generated in the topmost part of the particle are only detected with a probability of $W(\mathbf{r})=0.5$.

From the right column of Fig. 5, it is also obvious that the finite scattering length may result in a noticeable surface sensitivity when detecting the TEY of a nanoparticle. In the case of a nanoparticle with $D=12$ nm a large fraction of the volume is hardly probed [$W(\mathbf{r})$ close to 0]; the smaller particle, on the other hand, is more homogeneously probed with $W(\mathbf{r})\sim0.25$ in nearly the whole volume. The effect of saturation on TEY spectra of particles with $D=7.6$ nm is demonstrated in Fig. 6. Analogously to Fig. 4(a), the left panel shows the experimentally obtained isotropic spectra ($Y^+ + Y^-$) (dashed red line) together with the corrected Fe film data (solid black line). The right panel of Fig. 6 depicts the respective simulated TEY spectra with the same film data and reveals a good agreement of experiment and simulation, particularly in the vicinity of the L_3 edge, cf. the insets.

B. Correction factors for orbital and spin moments

By applying the sum rules on simulated TEY spectra we obtain the size-dependent magnetic spin and orbital moments $m_{\mathrm{spin}}^{\mathrm{eff,TEY}}$ and $m_{\mathrm{orb}}^{\mathrm{TEY}}$, respectively. The ratio of these moments and the moments $m_{\mathrm{spin}}^{\mathrm{eff},\mu}$ and m_{orb}^{μ} determined from the corrected data is shown in Fig. 7 by solid black and open red circles, respectively. In the range from 6 to 10 nm being of interest in the present work the values of $m_{\mathrm{orb}}^{\mathrm{TEY}}$ are reduced by a factor of 2 when compared to m_{orb}^{μ}. The spin moments $m_{\mathrm{spin}}^{\mathrm{eff,TEY}}$ show only a small decrease to about 95% of $m_{\mathrm{spin}}^{\mathrm{eff},\mu}$. The orbital moment determined from TEY spectra decreases further with increasing particle diameter and will show even negative values (not shown here). A similar behavior was also reported in the case of thin films in Ref. 26. Note that the ratios for the orbital moments presented in Fig. 7 may vary within about 10% for particles with diameters up to 10 nm when using different data sets (e.g., from a polycrystalline Fe film) in the calculation. The ratio for the spin moment is only slightly affected.

A small angular dependence of the correction factors has been observed by Fauth in Ref. 27, showing that the influence of saturation effects on the spin and orbital moments is slightly larger in grazing incidence. Since our experimental data have been recorded with a grazing angle of incidence being 30°, our calculations will slightly underestimate the effect of saturation.

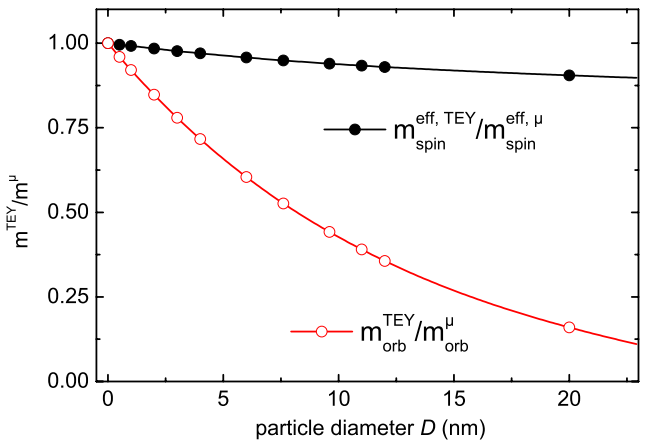

FIG. 7. (Color online) Size-dependent ratio of magnetic spin (solid black circles) and orbital moments (open red circles) determined from simulated TEY spectra of spherical Fe nanoparticles with diameter D and the respective moments obtained from the (corrected) absorption coefficients. Lines serve as a guide for the eyes.

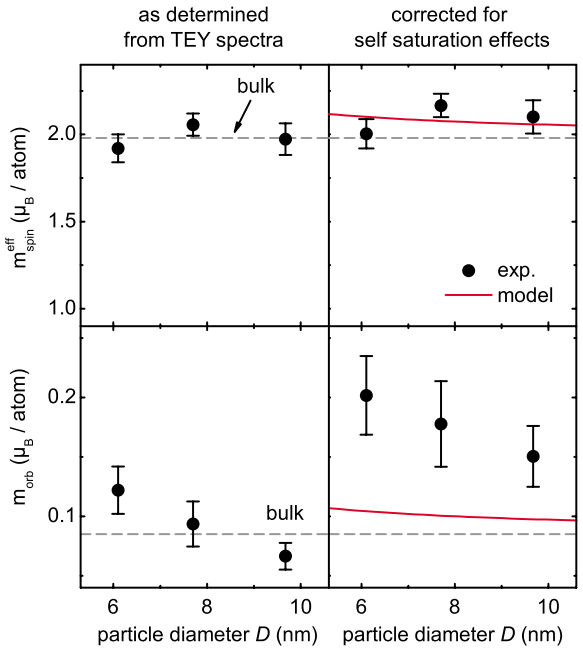

FIG. 8. (Color online) Size dependence of experimentally obtained magnetic spin $m_{\mathrm{spin}}^{\mathrm{eff}}$ (top panels) and orbital moments m_{orb} (panels at the bottom) of Fe nanoparticles after deposition onto Co/W(110). Left panels: evaluation from uncorrected TEY spectra; right side: after correcting for saturation effects. The corresponding Fe bulk values are indicated as dotted lines. The red lines depict model calculations assuming bulk and surface magnetic moments known from theoretical work on bulk iron.

VI. SIZE DEPENDENCE OF MAGNETIC SPIN AND ORBITAL MOMENTS

After discussing the simulations in Sec. V we now focus on the experimental data. In Fig. 8 magnetic spin and orbital moments of Fe nanoparticle ensembles are shown (solid black circles) for three different sizes: $D=6.1\pm0.5$ nm, $D=7.6\pm1.5$ nm, and $D=9.6\pm1.5$ nm supported on Co/W(110). The left panels depict the magnetic moments as obtained by analyzing uncorrected experimental TEY spectra. The magnetic spin moments (upper-left panel) show values close to the Fe bulk (dotted gray line) without a noticeable size dependence. In contrast the orbital moments (lower-left panel of Fig. 8) display a significant increase with decreasing particle size. Only the ensemble of the smallest particles shows a significantly enhanced magnetic orbital moment when compared to the corresponding bulk orbital moment, the largest particles even show slightly reduced orbital moments.

After correcting for the influence of electron-yield saturation effects (right panels of Fig. 8), the resulting spin moments (upper panel) are slightly enhanced when compared to the bulk value. At the same time the magnetic orbital moments (lower-right panel) are almost two times larger when compared to the initial (uncorrected) data or the respective bulk value. The increase in m_{orb} with decreasing particle size is conserved. The magnitude of the orbital moments is comparable to those found for much smaller Fe nanoparticles with diameters between 1 and 3 nm.[5,53] Fe clusters of this size consist of 200–700 atoms and thus possess a significant larger fraction of surface atoms when compared to the large nanoparticles in the present work. Since it is generally assumed that the enhancement of the magnetic moments scales with the fraction of surface atoms, the orbital moments in Fig. 8 appear surprisingly large.

TABLE II. Comparison of surface layer to volume contribution and the corresponding TEY contributions.

Particle diameter D (nm)	6.0	7.6	9.6
$V^{\mathrm{surf}}/V^{\mathrm{tot}}$	0.19	0.15	0.12
$\mathrm{TEY}^{\mathrm{surf}}/\mathrm{TEY}^{\mathrm{tot}}$	0.24	0.21	0.19

Therefore, the data are compared to a respective core shell model based on bulklike moments in the particle volume and enhanced spin and orbital moments at the particle surface. For the latter theoretically obtained values being reported for the bcc bulk Fe surface are used, i.e., a spin moment of $3.0\mu_B$ and an orbital moment of $0.2\mu_B$ per atom (cf. Ref. 54 and references therein).[55] The smaller differences found for the (001) and the (110) surfaces are neglected here. Taking further into account the above-determined particle shape, size-dependent average spin and orbital moments are obtained as depicted by the red curves in the upper- and lower-right panels of Fig. 8, respectively. The resulting spin moments are in agreement with the experimental data. However, the experimentally determined orbital moments are indeed still much larger than predicted by this simple model.

One explanation might be the enhanced surface sensitivity of TEY measurements. Assuming a surface shell of 0.2 nm, Eq. (1) yields the size-dependent surface contribution $\mathrm{TEY}^{\mathrm{surf}}$ to the total signal $\mathrm{TEY}^{\mathrm{tot}}$. The resulting ratios $\mathrm{TEY}^{\mathrm{surf}}/\mathrm{TEY}^{\mathrm{tot}}$ are compared to the ratios of the corresponding volume contributions $V^{\mathrm{surf}}/V^{\mathrm{tot}}$ in Table II. The surface contribution is overestimated in the TEY signal for the larger particles. For example, in the case of the 9.6 nm the surface shell contributes with 19% to the total TEY signal while it represents only 12% of the total particle volume. The surface sensitivity drops quite rapidly with decreasing particle size. For the smallest particles with $D=6.0$ nm the surface contribution to the TEY with 24% is only slightly larger than the respective surface shell contribution of 19% to the total particle volume.

Using the values given in Table II we can calculate the magnetic moments being required at the particle surface in order to explain the observed magnetic moments. Assuming bulklike properties in the particle volume the analysis reveals magnetic spin moments of about $\sim3.0\mu_B$ per atom at the particle surface, in good agreement with theory. For the surface orbital moments we find values between $\sim0.4\mu_B$ per atom for the largest and $\sim0.6\mu_B$ per atom for the smallest particles, clearly much larger than expected by theory. Orbital moments of this magnitude have been estimated for atoms at the edges of Fe nanostructures on Cu(111) and Au(111), respectively.[6,56] However, it seems unlikely that all surface atoms of the present nanoparticles have a similar low coordination even when incomplete surface facets may

greatly enhance the number of edge and vertex atoms. Instead, we believe that size-dependent strain in the nanoparticles modifies also the magnetic properties in the particle volume.

From thin films it is well known that strain (e.g., induced by misfit with respect to the substrate) can significantly alter their magnetic properties. In particular, strain can break the symmetry of the film lattice resulting, for instance, in tetragonal distortions as observed in Fe films on Pd(001).[57] The reduced symmetry may lead to a rise of the orbital moment being quenched in bcc lattice of bulk iron. Indeed, large magnetic orbital moments—being more than twice as large when compared to the bulk value—have been found by means of XMCD for the above mentioned body-centered-tetragonal (bct) iron films.[58,59] Remarkable strain may also be present in supported nanoparticles due to surface tension and the contact to the substrate.[17,60] Accordingly, a complex strain profile has recently been observed in a Pb nanoparticle by means of coherent x-ray diffraction.[61] The interfacial contact forces are determined by respective interface and surface energies of the system as well as by defects, step edges, and defects in the vicinity of the particles. If epitaxial order is possible at the interface, strain due to lattice mismatch has also to be taken into account, similar to islands or thin films grown by molecular-beam epitaxy on single crystalline substrates. Mesoscopic relaxations at the particle surface may additionally modify the magnetic properties.[62,63] A significant influence of the substrate and capping on the magnetic moments and magnetic anisotropy of supported nanoparticles in the present size regime has also been found in other experiments.[29,64–66] Finally, one may assume that all of the above mentioned phenomena are size-dependent and their impact on the magnetic properties will decrease with increasing particle size, similar to our observations on the magnetic orbital moments.

VII. CONCLUSION

Magnetic spin and orbital moments of mass-filtered Fe nanoparticles have been investigated by *in situ* performed XMCD measurements upon deposition onto hcp(0001) Co films on W(110). The presence of electron-yield saturation effects in the TEY spectra has been discussed and corrected based on respective numerical simulations. XMCD sum-rule analysis revealed bulklike spin moments but strongly enhanced magnetic orbital moments. HRTEM images yielded information on the shape and the crystallographic structure of the nanoparticles. Considering theoretical results on surface magnetism, we calculated the corresponding size dependence of the magnetic spin and orbital moments of the bcc nanoparticles with (001) and (110) surface facets. Even when taking into account the well-known enhancement of the magnetic moments at surfaces and the enhanced surface sensitivity when employing TEY detection, the calculated values cannot explain our experimental findings. Based on that, we conclude that the enhancement of the magnetic orbital moments may not be restricted to the outermost layer of the particles. Instead, we suppose that surface- and interface-induced strains break the cubic symmetry of the bcc lattice, resulting in a recovery of the orbital moment even within the particles. Mesoscopic relaxation effects at the surface facets could additionally lead to a remarkable distortion of the lattice in the first outermost layers.

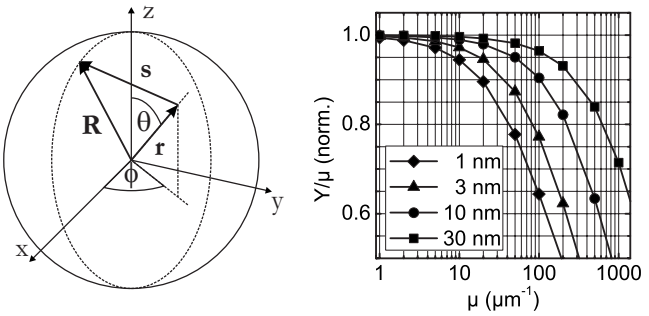

FIG. 9. Left: sketch of the vectors **R**, **r**, and **s** in a nanosphere that obey **R**=**r**+**s**. Right: deviation from a linear relation between Y and μ for four different particle sizes according to Eq. (A7).

ACKNOWLEDGMENTS

We gratefully acknowledge K. Fauth for valuable discussion on the TEY of deposited nanoparticles and V.S. Stepanyuk for his instructive comments on the magnetism of iron. Furthermore we thank R.-P. Mehtling, G. Holzhüter, and J. Carrey for characterization of nanoparticle deposits by transmission electron microscopy. Finally, we gratefully acknowledge technical assistance by the staff of BESSY and financial support by the Deutsche Forschungsgemeinschaft (DFG) via the priority program SPP 1153 Clusters in contact with surfaces within the Contracts No. KL 2188/1-3 and No. BA 1612/3-2 and -3.

APPENDIX: ON THE CALCULATION OF THE TOTAL ELECTRON YIELD OF A SUPPORTED NANOPARTICLE

The electron yield $dY(E,\mathbf{r})$ generated in the volume dV at site $\mathbf{r}$ of a particle is given by the product

$$dY(E,\mathbf{r}) = G\mu(E)I(E,\mathbf{r})W(\mathbf{r})dV, \tag{A1}$$

where G is the number of secondary electrons generated by one photon, $\mu(E)$ is the linear absorption coefficient, $I(E,\mathbf{r})$ is the local radiation intensity, and $W(\mathbf{r})$ is the probability that an electron excited at $\mathbf{r}$ is detected in a TEY experiment.[26,27] Both the calculation of $I(E,\mathbf{r})$ and $W(\mathbf{r})$ requires one to compute the distance from site $\mathbf{r}$ along any path $\mathbf{s}$ toward the boundary $\mathbf{R}$ of the particle with the radius R. Using spherical coordinates with the origin in the center of the sphere as depicted in the left part of Fig. 9, we can write

$$\mathbf{s}(s,\theta_s,\phi_s) = \mathbf{R}(R,\theta_R,\phi_R) - \mathbf{r}(r,\theta_r,\phi_r) \tag{A2}$$

and obtain the path length s as

$$s = \sqrt{r^2 f^2 - r^2 + R^2} - rf, \tag{A3}$$

with f being

$$f = (\sin\phi_r \sin\phi_s + \cos\phi_r \cos\phi_s)\sin\theta_s \sin\theta_r + \cos\theta_s \cos\theta_r. \quad \text{(A4)}$$

The local x-ray intensity in the particle $I(E,\mathbf{r})$ is then given by the Lambert-Beer law as

$$I(E,\mathbf{r}) = I_0 \exp[-s'\mu(E)], \quad \text{(A5)}$$

with I_0 being the incident intensity. The respective path length s' of the radiation is calculated using Eqs. (A3) and (A4) for photons impinging at θ_s' and ϕ_s'.

In order to calculate $W(\mathbf{r})$ we assume that the probability for an electron to leave the particle decreases exponentially with the distance of its excitation point to the surface.[24] Using a scattering length Λ_e the escape probability of *one* electron along a certain direction is then given by $\exp[-s/\Lambda_e]$ with s being the respective path length. In a total electron-yield experiment many electrons contribute to the signal. The isotropic nature of an Auger decay and the subsequent secondary electron excitation require then to average the escape probability over any emission angle θ_s and ϕ_s. Taking into account that only electrons escaping in the upper half sphere contribute to the TEY of supported nanoparticles, we can write

$$W(\mathbf{r}) = \frac{1}{4\pi}\int_0^{2\pi}\int_0^{\pi/2} \exp[-s/\Lambda_e]\sin\theta_s d\theta_s d\phi_s. \quad \text{(A6)}$$

Finally, we obtain the total electron yield by integrating Eq. (A1) over the particle volume,

$$Y(E) = G\mu(E)\int_0^{2\pi}\int_0^{\pi}\int_0^{R} I(E,\mathbf{r})W(\mathbf{r})r^2 \sin\theta_r dr d\theta_r d\phi_r. \quad \text{(A7)}$$

For the calculations presented in Sec. V (and in the right part of Fig. 9) we assumed perpendicularly incident light $\theta_s'=0$ and a constant conversion efficiency $G=1$. The experimentally observed effective escape depth of planar iron samples ($\lambda_e=1.7$ nm) is reproduced in respective simulations by using $\Lambda_e=1.67\lambda_e$. Accordingly, the scattering length has been set to $\Lambda_e=2.84$ nm. The integrals have been evaluated numerically using an adaptive quadrature method and have been validated by means of Monte Carlo simulations similar to those described in Ref. 27.

The electron-yield saturation effects are given by the integral term in Eq. (A7). The right part of Fig. 9 shows the resulting ratio Y/μ for iron nanospheres with different diameters being normalized to 1 in the limit $\mu\to 0$ (cf. Ref. 27). The considered range of μ covers the L edges of iron.

*Present address: Paul Scherrer Institute, CH-5232 Villigen, Switzerland.

[1] H. Haberland, *Clusters of Atoms and Molecules* (Springer, Berlin, 1995).
[2] J. P. Bucher, D. C. Douglass, and L. A. Bloomfield, Phys. Rev. Lett. **66**, 3052 (1991).
[3] I. M. L. Billas, J. A. Becker, A. Châtelain, and W. A. de Heer, Phys. Rev. Lett. **71**, 4067 (1993).
[4] I. M. L. Billas, A. Châtelain, and W. A. de Heer, Science **265**, 1682 (1994).
[5] K. W. Edmonds, C. Binns, S. H. Baker, S. C. Thornton, C. Norris, J. B. Goedkoop, M. Finazzi, and N. B. Brookes, Phys. Rev. B **60**, 472 (1999).
[6] P. Ohresser, G. Ghiringhelli, O. Tjernberg, N. B. Brookes, and M. Finazzi, Phys. Rev. B **62**, 5803 (2000).
[7] J. T. Lau, A. Föhlisch, R. Nietubyc, M. Reif, and W. Wurth, Phys. Rev. Lett. **89**, 057201 (2002).
[8] H. A. Dürr, S. S. Dhesi, E. Dudzik, D. Knabben, G. van der Laan, J. B. Goedkoop, and F. U. Hillebrecht, Phys. Rev. B **59**, R701 (1999).
[9] T. Koide, H. Miyauchi, J. Okamoto, T. Shidara, A. Fujimori, H. Fukutani, K. Amemiya, H. Takeshita, S. Yuasa, T. Katayama, and Y. Suzuki, Phys. Rev. Lett. **87**, 257201 (2001).
[10] J. Bansmann, S. H. Baker, C. Binns, J. A. Blackman, J. P. Bucher, J. Dorantes-Dávila, V. Dupuis, L. Favre, D. Kechrakos, A. Kleibert, K.-H. Meiwes-Broer, G. M. Pastor, A. Perez, O. Toulemonde, K. N. Trohidou, J. Tuaillon, and Y. Xie, Surf. Sci. Rep. **56**, 189 (2005).
[11] P. Gambardella, S. Rusponi, M. Veronese, S. S. Dhesi, C. Grazioli, A. Dallmeyer, I. Cabria, R. Zeller, P. H. Dederichs, K. Kern, C. Carbone, and H. Brune, Science **300**, 1130 (2003).
[12] V. F. Puntes, K. M. Krishnan, and A. P. Alivisatos, Science **291**, 2115 (2001).
[13] F. Baletto and R. Ferrando, Rev. Mod. Phys. **77**, 371 (2005).
[14] D. Gerion, A. Hirt, I. M. L. Billas, A. Châtelain, and W. A. de Heer, Phys. Rev. B **62**, 7491 (2000).
[15] G. Rollmann, M. E. Gruner, A. Hucht, R. Meyer, P. Entel, M. L. Tiago, and J. R. Chelikowsky, Phys. Rev. Lett. **99**, 083402 (2007).
[16] O. Kitakami, H. Sato, Y. Shimada, F. Sato, and M. Tanaka, Phys. Rev. B **56**, 13849 (1997).
[17] B. Gilbert, F. Huang, H. Zhang, G. A. Waychunas, and J. F. Banfield, Science **305**, 651 (2004).
[18] R.-P. Methling, V. Senz, E.-D. Klinkenberg, Th. Diederich, J. Tiggesbäumker, G. Holzhüter, J. Bansmann, and K.-H. Meiwes-Broer, Eur. Phys. J. D **16**, 173 (2001).
[19] J. Passig, K.-H. Meiwes-Broer, and J. Tiggesbäumker, Rev. Sci. Instrum. **77**, 093304 (2006).
[20] A. Kleibert, J. Bansmann, J. Passig, M. Getzlaff, and K.-H. Meiwes-Broer, J. Appl. Phys. **101**, 114318 (2007).
[21] A. Kleibert, F. Bulut, R. K. Gebhardt, W. Rosellen, D. Sudfeld, J. Passig, J. Bansmann, K.-H. Meiwes-Broer, and M. Getzlaff, J. Phys.: Condens. Matter **20**, 445005 (2008).
[22] J. Stöhr, J. Magn. Magn. Mater. **200**, 470 (1999).
[23] H. Wende, Rep. Prog. Phys. **67**, 2105 (2004).
[24] J. Stöhr, in *NEXAFS Spectroscopy*, Springer Series in Surface Sciences Vol. 25 (Springer, Berlin, 1992).
[25] J. H. Dunn, D. Arvanitis, N. Mårtensson, M. Tischer, F. May, M. Russo, and K. Baberschke, J. Phys.: Condens. Matter **7**, 1111 (1995).

[26] R. Nakajima, J. Stöhr, and Y. U. Idzerda, Phys. Rev. B **59**, 6421 (1999).
[27] K. Fauth, Appl. Phys. Lett. **85**, 3271 (2004).
[28] J. Bansmann, Appl. Phys. A: Mater. Sci. Process. **72**, 447 (2001).
[29] J. Bansmann, M. Getzlaff, A. Kleibert, F. Bulut, R. K. Gebhardt, and K.-H. Meiwes-Broer, Appl. Phys. A: Mater. Sci. Process. **82**, 73 (2006).
[30] J. Stöhr and H. König, Phys. Rev. Lett. **75**, 3748 (1995).
[31] C. T. Chen, Y. U. Idzerda, H.-J. Lin, N. V. Smith, G. Meigs, E. Chaban, G. H. Ho, E. Pellegrin, and F. Sette, Phys. Rev. Lett. **75**, 152 (1995).
[32] More precisely, the size distribution is given by a log-normal function. However, for the present purpose a Gaussian yields a more intuitive and still precise understanding of the ensemble properties.
[33] J. Bansmann and A. Kleibert, Appl. Phys. A: Mater. Sci. Process. **80**, 957 (2005).
[34] H. Fritzsche, J. Kohlhepp, and U. Gradmann, Phys. Rev. B **51**, 15933 (1995).
[35] A. Kleibert, V. Senz, J. Bansmann, and P. M. Oppeneer, Phys. Rev. B **72**, 144404 (2005).
[36] M. Bode, R. Pascal, and R. Wiesendanger, Surf. Sci. **344**, 185 (1995).
[37] A. Bettac, J. Bansmann, V. Senz, and K.-H. Meiwes-Broer, Surf. Sci. **454-456**, 936 (2000).
[38] N. Combe, P. Jensen, and A. Pimpinelli, Phys. Rev. Lett. **85**, 110 (2000).
[39] N. Lümmen and T. Kraska, Phys. Rev. B **71**, 205403 (2005).
[40] T. Vystavel, G. Palasantzas, S. A. Koch, and J. Th. M. De Hosson, Appl. Phys. Lett. **82**, 197 (2003).
[41] G. Wulff, Z. Kristallogr. **34**, 449 (1901).
[42] L. Vitos, A. V. Ruban, H. L. Skriver, and J. Kollár, Surf. Sci. **411**, 186 (1998).
[43] R.-P. Methling, Ph.D. thesis, Rostock University, 2004.
[44] J. T. Lau, J. Rittmann, V. Zamudio-Bayer, M. Vogel, K. Hirsch, P. Klar, F. Lofink, T. Moller, and B. v. Issendorff, Phys. Rev. Lett. **101**, 153401 (2008).
[45] B. T. Thole, P. Carra, F. Sette, and G. van der Laan, Phys. Rev. Lett. **68**, 1943 (1992).
[46] D. Weller, J. Stöhr, R. Nakajima, A. Carl, M. G. Samant, C. Chappert, R. Mégy, P. Beauvillain, P. Veillet, and G. A. Held, Phys. Rev. Lett. **75**, 3752 (1995).
[47] P. Bruno, Phys. Rev. B **39**, 865 (1989).
[48] P. Carra, B. T. Thole, M. Altarelli, and X. Wang, Phys. Rev. Lett. **70**, 694 (1993).
[49] T. Oguchi and T. Shishidou, Phys. Rev. B **70**, 024412 (2004).
[50] H. J. Elmers and U. Gradmann, Appl. Phys. A: Solids Surf. **51**, 255 (1990).
[51] U. Gradmann and G. Waller, Surf. Sci. **116**, 539 (1982).
[52] For sum-rule application, a steplike continuum contribution is subtracted from the averaged spectra (dotted gray line in the left part of Fig. 4) and a bulklike number of $3d$ holes (n_h=3.49) is assumed (Ref. 31).
[53] S. H. Baker, C. Binns, K. W. Edmonds, M. J. Maher, S. C. Thornton, S. Louch, and S. S. Dhesi, J. Magn. Magn. Mater. **247**, 19 (2002).
[54] O. Šipr, M. Košuth, and H. Ebert, Phys. Rev. B **70**, 174423 (2004).
[55] Please note that magnetic orbital moments are underestimated by relativistic density-functional theory (Ref. 54). However, it has been shown that including a so-called orbital polarization (OP) term in respective calculations allows one to reproduce experimental bulk and surface data very well (Ref. 67). Our model calculations thus rely on values that take the OP term into account. A common result of surface magnetism theory is that the most significant enhancement of the orbital moment is restricted to the uppermost surface layer. Accordingly, our model considers only an enhancement in the outermost layer of the nanoparticles.
[56] P. Ohresser, N. B. Brookes, S. Padovani, F. Scheurer, and H. Bulou, Phys. Rev. B **64**, 104429 (2001).
[57] H. L. Meyerheim, R. Popescu, and J. Kirschner, Phys. Rev. B **73**, 245432 (2006).
[58] X. Le Cann, C. Boeglin, B. Carrière, and K. Hricovini, Phys. Rev. B **54**, 373 (1996).
[59] C. Boeglin, H. Bulou, J. Hommet, X. Le Cann, H. Magnan, P. Le Fèvre, and D. Chandesris, Phys. Rev. B **60**, 4220 (1999).
[60] The actual strain will certainly depend on the materials being combined as well as on the orientation of the particles with respect to the substrate. Thus, the HRTEM investigations on Fe nanoparticles embedded in Al being presented in Sec. III do not allow one to draw conclusions on the strain profile of Fe particles supported by a Co/W(110) substrate.
[61] M. A. Pfeifer, G. J. Williams, I. A. Vartanyants, R. Harder, and I. K. Robinson, Nature (London) **442**, 63 (2006).
[62] O. V. Lysenko, V. S. Stepanyuk, W. Hergert, and J. Kirschner, Phys. Rev. Lett. **89**, 126102 (2002).
[63] W. J. Huang, R. Sun, J. Tao, L. D. Menard, R. G. Nuzzo, and J. M. Zuo, Nature Mater. **7**, 308 (2008).
[64] F. Luis, F. Bartolomé, F. Petroff, J. Bartolomé, L. M. García, C. Deranlot, H. Jaffrès, M. J. Martínez, P. Bencok, F. Wilhelm, A. Rogalev, and N. B. Brookes, Europhys. Lett. **76**, 142 (2006).
[65] J. P. Pierce, M. A. Torija, Z. Gai, Junren Shi, T. C. Schulthess, G. A. Farnan, J. F. Wendelken, E. W. Plummer, and J. Shen, Phys. Rev. Lett. **92**, 237201 (2004).
[66] S. H. Baker, M. Roy, S. J. Gurman, S. Louch, A. Bleloch, and C. Binns, J. Phys.: Condens. Matter **16**, 7813 (2004).
[67] O. Hjortstam, J. Trygg, J. M. Wills, B. Johansson, and O. Eriksson, Phys. Rev. B **53**, 9204 (1996).